Journal of Power Sources 243 (2013) 88–94

Contents lists available at SciVerse ScienceDirect

Journal of Power Sources

journal homepage: www.elsevier.com/locate/jpowsour

Carbon nanotubes as support of well dispersed platinum nanoparticles via colloidal synthesis

B. Escobar [a], R. Barbosa [b], M. Miki Yoshida [c], Y. Verde Gomez [a,*]

[a] Instituto Tecnológico de Cancún, Av. Kabah km 3, Cancún, Quintana Roo 77500, Mexico
[b] Universidad de Quintana Roo, Boulevard Bahía s/n, Chetumal, Quintana Roo 77019, Mexico
[c] Centro de Investigación en Materiales Avanzados S.C., Laboratorio Nacional de Nanotecnología, Miguel de Cervantes 120, Chihuahua, Chih. 31109, Mexico

HIGHLIGHTS

- The Pt nanoparticles shows spherical shape with a good distribution.
- Pt colloidal nanoparticles were supported onto carbon nanotubes.
- The size of the Pt nanoparticles was between 6.1 ± 0.85 and 6.5 ± 1.5 nm.
- X-ray diffraction shows diffraction peaks corresponding to graphite and metallic Pt.
- Electrocatalytic activity of Pt/MWCNT was higher than the Pt/C.

GRAPHICAL ABSTRACT

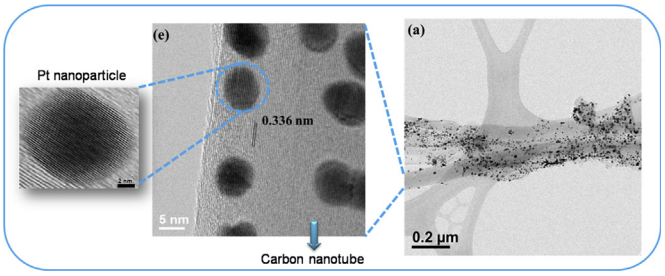

ARTICLE INFO

Article history:
Received 21 December 2012
Received in revised form
23 April 2013
Accepted 24 May 2013
Available online 6 June 2013

Keywords:
Carbon nanotubes
Colloidal dispersion
Pt/MWCNT
Electron microscopy
Electrochemical active area
Fuel cells

ABSTRACT

Pt colloidal nanoparticles were synthesized by simultaneous chemical reduction of metallic salts in presence of poly (N-vinyl-2-pyrrolidone) as protecting agent. The uniform and highly ordered Pt colloidal nanoparticles were associated to well dispersed particles ranging in particle size distribution around 4.5 ± 1.9 nm. The nanoparticles were deposited onto multiwalled carbon nanotubes (MWCNT). MWCNT were synthesized by chemical vapor deposition (CVD) method. Before the metal impregnation, the MWCNT were treated with HNO_3 in reflux. Prepared Pt catalyst were characterized by various physical and electrochemical techniques, that is, X-ray diffraction (XRD), high resolution transmission electron microscopy (HRTEM), scanning electron microscopy (SEM), energy dispersive X-ray spectroscopy (EDS), Raman spectroscopy and cyclic voltammetry (CV). Raman spectroscopy reveals changes intensity ratio IG′/IG in the samples, after the cleaning process and Pt loading, indicating changes in the crystallinity of the materials. HRTEM showed Pt particles between 6.1 ± 0.9 nm and 6.5 ± 1.5 nm are well dispersed along the carbon nanotubes. XRD patterns show characteristics peaks corresponding to graphite and metallic Pt. The electrochemical properties of the MWCNT supported Pt nanoparticles were investigated by analyzing the response of the nanostructured catalyst for cyclic voltammetry and compared with a commercial material.

1. Introduction

The synthesis of noble metal nanoparticles, particularly Pt, has been a growing field of interest in recent years. Due to their optimal physicochemical characteristics, these kinds of nanoparticles have been utilized in several technological applications such as catalysts, sensors, optical devices, etc. [1–3]. Good quality colloidal

* Corresponding author. Tel.: +52 998 8807432x1002; fax: +52 998 8807433.
E-mail addresses: yverde@itcancun.edu.mx, ysmaelverde@yahoo.com (Y. Verde Gomez).

0378-7753/$ – see front matter © 2013 Elsevier B.V. All rights reserved.
http://dx.doi.org/10.1016/j.jpowsour.2013.05.123

nanoparticles can be produced using different reactants, as well as reduction methodologies as thermal [4], photochemical [5], electrochemical [6] and chemical [7–9]. However, only some of these methods ensure the synthesis of materials with good control on the size and particle distribution. The chemical reduction method has advantages compared to others in the synthesis of metal nanoparticles. This method is simple and reproducible, and is possible to obtain homogeneous and nanometer scale particles (<10 nm) [10]. Furthermore, structure, shape and particle size can be controlled simply by varying the preparation conditions. The synthesis of nanoparticles with good dispersion is a first step to obtained nanomaterials with high catalytic activity in various electrochemical reactions. The next step would be support these colloidal dispersions on nanostructured carbon in order to obtain well-dispersed nanoparticles. The supporting material as well as the nanoparticles synthesis, have a direct influence to provide dispersion, stability and in consequence, a possible good electroactivity in the reactions of a fuel cell.

Platinum has attracted important attention because it is a stable and excellent catalyst for many purposes, such as its application in PEM fuel cells as cathode for the oxygen reduction reaction at relatively low temperature. It is well known that the Pt catalytic activity strongly depends on the particle shape, size and size distribution [11], as well as the support, which determines the degree of dispersion of the catalyst. It has been reported that the best electroactivity performance of Pt/C were obtained with particles in the range of 2–5 nm, and carbon particles in the range of 30–100 nm in diameter [12]. Pt nanostructured supporting material most commonly used is carbon black and activated carbons, with Vulcan XC-72 being the most representative. These conventional carbonous materials have been investigated in long time performance tests. It was found that carbon blacks get oxidized in a fuel cell environment, promoting the agglomeration of Pt and decreasing in consequence the electrocatalytic activity. Therefore, the catalysts durability is a critical issue to be resolved for the commercialization of the PEMFC [13]. Carbon nanotubes (CNTs) are attractive materials for catalyst support in PEMFC because of their morphology and interesting properties such as nanometric size, highly accessible surface area, excellent corrosion resistance, good electrical conductivity, and high stability, compared to conventional carbon black powders [14]. The deposition of Pt metal nanoparticles on CNTs has resulted in a higher catalytic activity compare to carbon black support [15,16]. However, the high dispersion of Pt nanoparticles with controlled loading is still a challenge due to the inert surfaces of CNTs [17]. The deposition of Pt over CNTs can be achieved via diverse procedures such as, chemical vapor deposition [18], microwave-assisted polyol process [19], electrodeposition method [20], chemical reduction [21], wet chemistry impregnation [22] and hydrothermal method [23] among others. This paper reports the colloidal synthesis of Pt nanoparticles by chemical reduction method in presence of poly(-vinylpyrrolidone) [24,25] and $NaBH_4$ [26,27]; and their support on MWCNTs synthesized by chemical vapor deposition (CVD). The structural and morphological properties as well as the electrochemical characterization of the materials are presented.

2. Experimental section

2.1. Multi-walled carbon nanotubes synthesis

The MWCNTs used as support were obtained by CVD method using Vycor tubing as substrate. The precursor solution was a mixture of catalyst (1.9 g ferrocene, 98% from Aldrich) and toluene (25 ml, 99.8% from J.T. Baker). Argon gas (99.998% purity) was used to carry the precursor mixture into the Vycor tubing placed inside a tubular furnace at 1173 K. After the MWCNT synthesis, the system was allowed to cool down at room temperature. MWCNTs inside the Vycor tubing were mechanically removed. Acid treatment is a well-accepted process not only to clean MWCNTs but also to functionalizing them, incorporating carboxyl and hydroxide groups which improves the anchoring of Pt ions [17,28]. The MWCNTs were purified to remove residual iron and functionalized in a reflux system with 30% H_2O_2 (30% from J.T. Baker) and HNO_3 (66.5% from J.T. Baker) by 2 h, and 24 h respectively at 373 K. Finally, the MWCNTs were washed several times with triple distilled water (from J.T. Baker).

2.2. Synthesis of MWCNT supported Pt nanoparticles

Colloidal dispersions of Pt nanoparticles were prepared as previously reported by the authors [10]; different amounts of platinum tetrachloride (99.99% from Aldrich) were dispersed in methanol (1.0 mmol dm^{-3} and 5.1 mmol dm^{-3}), then, 30 mg of poly (N-vinil-2-pirrolidone) (PVP, 99.9% from Aldrich) was added to 25 ml of the metal ion solution as the capping agent. A stable homogeneous dark brown colored colloidal dispersion was formed after adding 1 ml of a 0.044 mol dm^{-3} solution of $NaBH_4$ (98.7% from Fermont).

Pt nanoparticles supported on MWCNTs were prepared as follows; 100 mg of MWCNTs were dispersed in methanol with strongly ultrasonication for about 1 h. Afterward, the Pt colloidal dispersion was added and vigorously stirred during 30 min. Two samples with different Pt loading were tried, with concentrations of 1.0 and 5.1 mmol dm^{-3} for samples of 10 wt.% (Pt10) and 20 wt.% (Pt20), respectively. Then they were dried at around 393 K until the solution was completely evaporated. Finally, anchoring of Pt nanoparticles on the carbon nanotubes surface was carried out by a thermal process in a tubular furnace adapted with a quartz tube, where samples were annealed at 623 K under nitrogen atmosphere for 30 min with a flow rate of 50 ml min^{-1}.

2.3. Characterization

The samples were characterized by X-Ray Diffraction (XRD) in a Panalytical Xpert system using Cu Kα radiation at 40 kV and 30 mA, the scanning angle 2θ was varied between 20° and 80°, at 0.1° min^{-1}.

High Resolution Scanning Electron Microscopy analyses (HRSEM) were performed with a field emission scanning electron microscope JEOL JSM-7401F operated at low voltage. To determine the catalysts compositions, energy dispersive X-ray spectroscopy analysis (EDS) was done with a Bruker detector attached to a Tescan Vega 3 scanning electron microscope with an operating voltage of 20 kV. High resolution transmission electron micrographs were obtained in a JEOL JEM-2200FS transmission electron microscope at 200 kV, in order to get information about the mean particle size and distribution of Pt on colloidal solution and Pt on MWCNTs, respectively. In order to get the nanomaterials structure, Raman spectroscopy measurements were carried out using a Horiba Jobin Yvon model LabRam HR VIS. In addition, thermogravimetric analyses were carried out in a TGA Q500 instrument, in air from room temperature to 1223 K using a heating ramp of 283 K min^{-1}.

On the other hand, all electrochemical experiments were performed in a conventional three-electrode test cell at room temperature. An Ag/AgCl (saturated KCl) electrode and a platinum wire were used as reference and counter electrodes respectively, and 0.5 M H_2SO_4 as electrolyte. The working electrode was a thin layer catalyst supported on a glassy carbon electrode. The previously polished working electrode had an area of approximately 0.071 cm^2. The electrochemical active area of the sample was determined by cyclic voltammetry analyses using a BAS RDE-2 potentiostat/galvanostat instrument with a scan rate of 20 mV s^{-1}.

3. Results and discussion

3.1. SEM analyses

MWCNTs and Pt nanoparticles supported on MWCNTs (Pt/MWCNTs) were analyzed by field emission SEM. The MWCNTs forest obtained have a thickness around 1 mm, with diameters between 60 and 100 nm.

EDS analyses of the MWCNTs showed 4 wt.% of iron before purification and functionalization process. After the previously mentioned processes, the Fe percentage present in the MWCNTs was about 2.5 wt.% due to the iron that remains inside the MWCNTs, indicating the high yield of the synthesis procedure.

The scanning electron micrographs of Pt nanoparticles supported on MWCNTs are shown in Fig. 1a and b, for samples Pt10 and Pt20, respectively. The images clearly show the surface of the MWCNTs decorated with Pt (bright particles), which are uniformly distributed along carbon nanotubes. Statistical EDS analysis of several random locations on the samples, showed Pt contents of 8.3 wt.% and 19.7 wt.% for Pt10 and Pt20 respectively which, this is in agreement with the theoretical Pt loading (10 wt.% and 20 wt.%).

3.2. TEM analyses

TEM analysis was performed for the colloidal dispersion of Pt and for the Pt nanoparticles supported on MWCNTs, samples Pt10 and Pt20. For the study of the Pt colloidal dispersion, a drop of colloidal sample was deposited on a carbon coated grid and dried in vacuum. Fig. 2 displays typical TEM micrographs of Pt colloids prepared by chemical reduction method; the particles exhibit a narrow particle size distribution (2–5 nm) with some agglomeration.

The average particle size and the standard deviation were obtained by measuring the diameter of a large number of particles. The average particle size was estimated about 4.5 nm ± 1.9 nm. Peuckert et al. [29] and Stonehart [30] propose that the optimum Pt particle size for the oxygen reduction reaction should lie between 3 and 5 nm. Then the nanoparticle obtained was within the optimal range for a good electrochemical performance of the catalyst in application as electrode in PEMFC.

Results obtained by TEM analysis for colloidal Pt10 and Pt20 supported on CNT can be seen in Fig. 3. Fig. 3a and b show bright field STEM images of samples Pt10 and Pt20, respectively. Fig. 3c and d show dark field images of the same samples. Also, Fig. 3d and f show high resolution STEM images of the respective samples. The particles show spherical shape with a good distribution along the carbon nanotubes surface. The analysis was performed in different and random areas of the sample, observing always a very well and uniform distribution of Pt nanoparticles on MWCNTs. The metallic particles size distribution was obtained by directly measuring the size taking a large amount of particles in randomly areas of the TEM images. The corresponding particle size distribution histograms are reported in Fig. 4. As it can be seen, the average particle size is about 6.1 nm and 6.5 nm for Pt10 and Pt20, respectively. Generally, the particle size increases and the size distribution broadens with the increase in platinum loading [8]; however the particle sizes obtained can be suitable as electrocatalyst fuel cell. The slight increment of the Pt particle size (colloidal sample) after deposition can be attributed to the thermal reduction process during the synthesis of Pt/MWCNT which agglomerates the nanoparticles.

3.3. XRD analyses

Carbon nanotubes formation is also confirmed from the XRD pattern shown in Fig. 5, with the typical peaks for carbon nanotubes at 26.22° and 53.97° 2θ which corresponds to the (002) and (004) planes of graphite 2H (from the crystallographic chart 01-070-2057

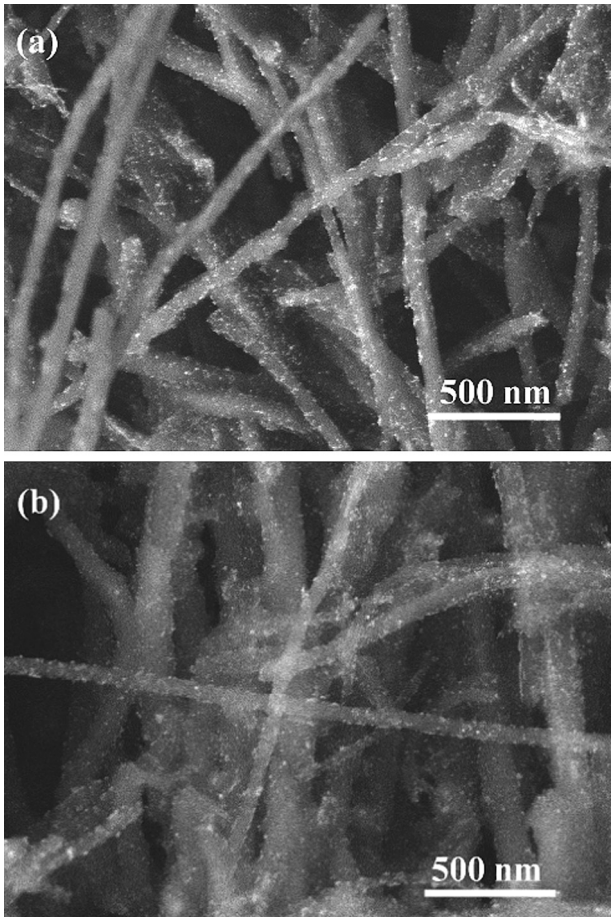

Fig. 1. SEM micrographs of Pt nanoparticles supported on MWCNTs catalysts, a) Pt10 and b) Pt20.

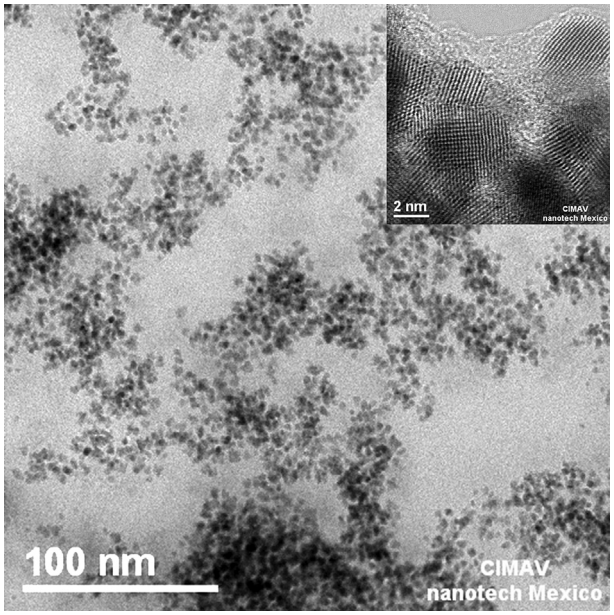

Fig. 2. TEM micrographs of Pt nanoparticles of colloidal dispersion, an inset shows particles around 4 nm at high resolution.

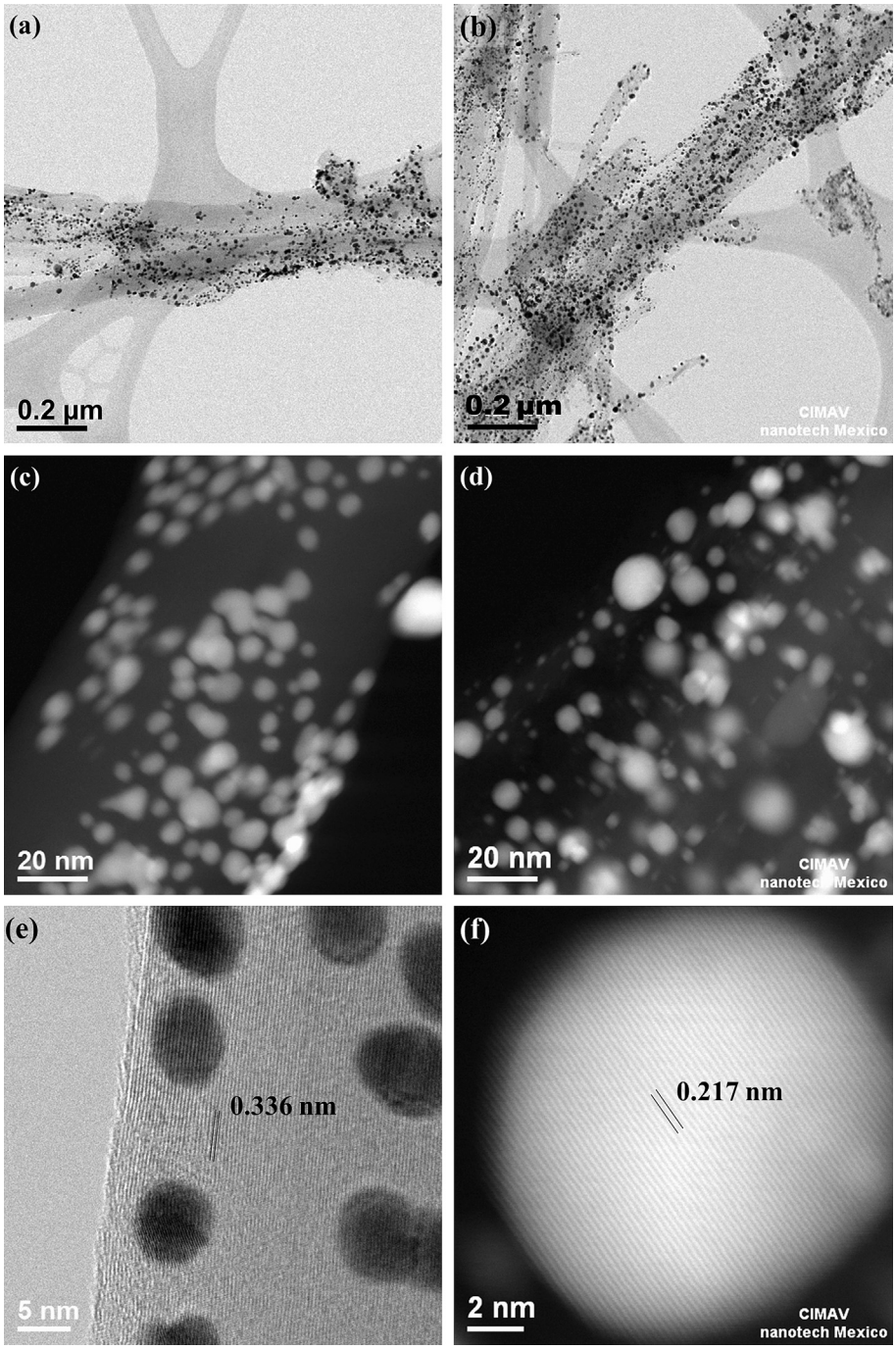

Fig. 3. TEM micrographs of Pt/MWCNTs a) bright field c) dark field, and e) high resolution corresponding to Pt10; and b) bright field, d) dark field and f) high resolution particle to sample Pt20.

of the International Center for Diffraction Data, ICDD), respectively. The presence of a peak around 32° is attributed to residual sodium chloride. The typical diffraction peaks which belong to FCC platinum can be clearly observed for both samples. The characteristic peaks of metallic Pt nanoparticles (111), (200) and (220), indicate that Pt has been reduced successfully.

3.4. TGA

The thermogravimetric analyses (TGA) were carried out under oxygen flow from 293 to 973 K at 283 K min^{-1} heating rate. The plots of samples Pt10 and Pt20 are shown in Fig. 6, where the carbon samples decomposition takes place roughly between 573 and 823 K. After carbon consumption, the residuals materials were around of 12% and 21% (samples Pt10 and Pt20, respectively). This difference in the amount of residual material and metal loading (only Pt) is due to the presence of iron, which is present in the samples. This result is in agreement with the tailor experimental Pt loading.

3.5. Raman spectroscopy

Raman spectroscopy is a powerful method for determining the degree of structural ordering or the presence of contaminants [31]. Tests were performed for samples of raw MWCNTs (DF1), the

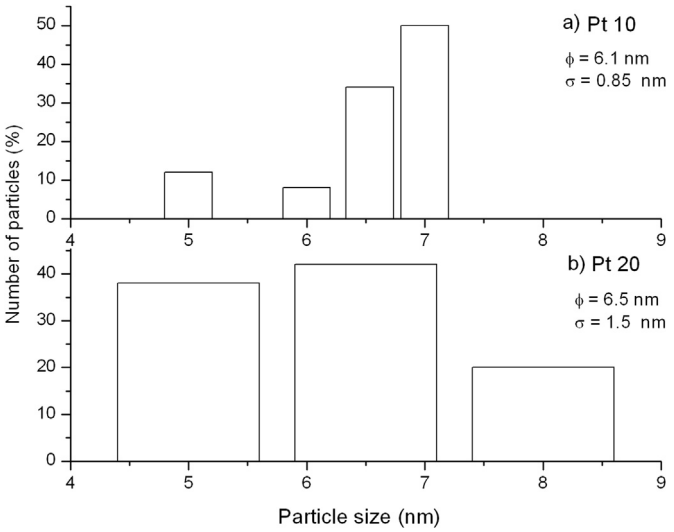

Fig. 4. Particle size distribution, a) Pt10 and b) Pt20.

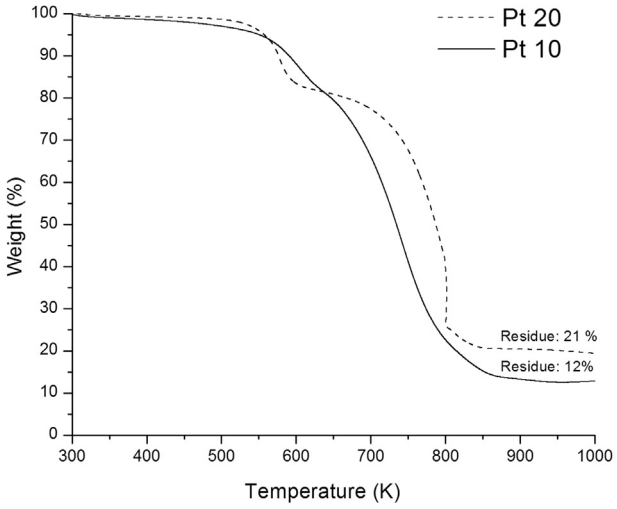

Fig. 6. Thermogravimetric analysis for Pt10 and Pt20.

purified MWCNTs (DFL1) and Pt on MWCNTs, Pt10 and Pt20. Fig. 7 shows all the spectra having strong bands at 1330 cm^{-1} and 1575 cm^{-1} corresponding to the D and G bands, respectively. The D band is the A_{1g} symmetrical stretch originated from crystalline disorders and lattice imperfections in the CNT (pentagons, heptagons, etc.). These defects can facilitate the anchoring of the Pt nanoparticles on MWCNTs surface [32]. The G band is assigned to the tangential stretching mode of highly oriented graphite with E_{2g} symmetry, which is the high frequency. These two well-defined bands are detected in the first-order section of the spectra. The features observed at 2660 cm^{-1}, the second-order section, correspond to the G′ band which is an overtone of the D band and is very sensitive to the stacking order of the graphene sheets [33,34].

The intensity ratio ID/IG (measurement of the structural disorder originated by the defects formation) and IG′/IG (average degree of crystalline perfection) are shown in Table 1.

DF1 sample has an average value I_D/I_G of 1.00 ± 0.01 representing the presence of amorphous carbon, after the purification process this value is reduced to 0.67 ± 0.01 due to the reduction of the amount of iron and amorphous carbon in the sample which indicate the structural defects reducing and the crystallinity increment. On the other hand, the intensity ratio $I_{G'}/I_G$ shows that the smoothing of MWCNTs increases 0.54 ± 0.01 and 0.86 ± 0.02 for the sample DFL1 and DF1, respectively. This is due to the decrease of amorphous carbon removed during the cleaning process. The decrease in the intensity ratio $I_{G'}/I_G$ after Pt deposit up to 0.80 ± 0.03 in Pt10 sample is due to the presence of the nanoparticles, which are adhered to the walls of carbon nanotubes leading to the catalyst being less smooth. This effect is most evident in the sample Pt20 where $I_{G'}/I_G$ is 0.31 ± 0.02.

3.6. Electroactive area

It is accepted that the electroactive area of Pt electrode can be determined from the charge of adsorption and desorption of hydrogen atoms measured by cyclic voltammetry in aqueous solution. The electrochemically active area (EAA) for Pt/MWCNTs, and commercial catalysts (Pt/Vulcan), was estimated using cyclic voltammetric measurements with a scan rate of 20 mV s^{-1} from −0.2 V to 0.6 V vs Ag/AgCl (Sat KCl). The working electrodes have a platinum loading of 0.1 mg cm^{-2}.

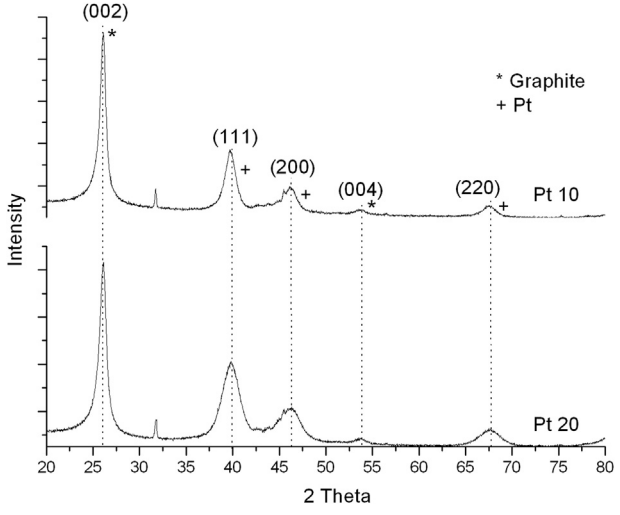

Fig. 5. X-ray diffraction patterns of Pt/MWCNTs synthesized.

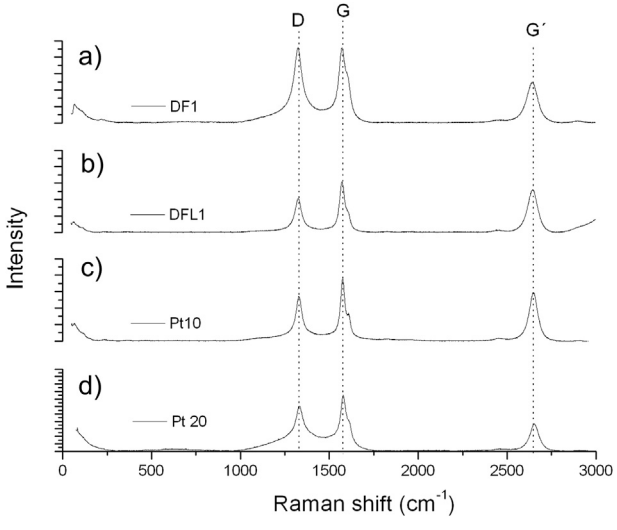

Fig. 7. Raman spectroscopy, a) MWCNTs as obtained, b) purified MWCNTs, c) Pt10 and d) Pt20.

Table 1
Intensity ratio of peaks from raw MWCNTs (DF1), purified MWCNTs (DFL1) and MWCNTs supported Pt nanoparticles, (Pt10 and Pt20).

Sample	I_D/I_G	$I_{G'}/I_G$
DF1	1.00 ± 0.01	0.54 ± 0.01
DFL1	0.67 ± 0.01	0.86 ± 0.02
Pt10	0.72 ± 0.03	0.80 ± 0.03
Pt20	0.84 ± 0.01	0.31 ± 0.02

Fig. 8 shows the cyclic voltammograms of the samples, colloidal synthesized Pt/MWCNT (Pt10 and Pt20) and commercial Pt/Vulcan (Pt10/Vulcan and Pt20/Vulcan). Electrochemical performance of Pt/MWCNT of Pt10 and Pt20 shows higher activity than the commercial, corroborated by EAA analysis. The characteristic peaks in the negative region (−0.2–0 V vs Ag/AgCl (Sat KCl)) are attributed to the atomic hydrogen adsorption on the Pt surface and reflected the electrochemically active area. The more negative potential peak is associated with H_2 adsorption on Pt plane (100).

The EAA was calculated using Equation (1) and integrating the voltammograms curves in Fig. 8:

$$\mathrm{EAA} = Q/\mu_{\mathrm{Pt}}L \quad (1)$$

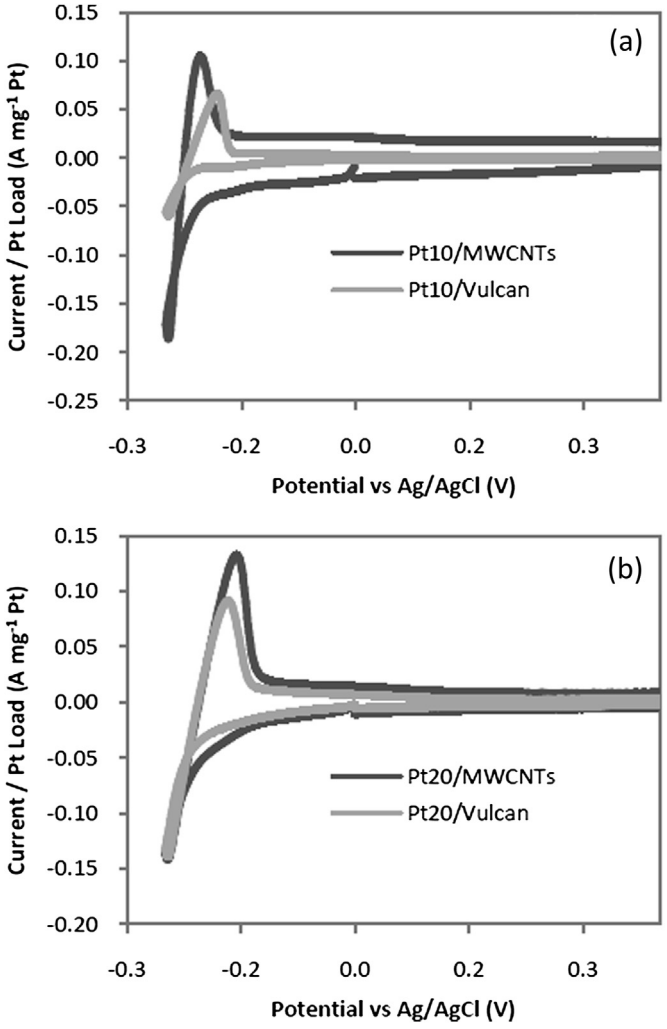

Fig. 8. Cyclic voltammetry in a 0.5 M H_2SO_4 solution electrolyte, at 20 mV/s scan rate in nitrogen atmosphere. a) Pt10 and Pt10/Vulcan; b) Pt20 and Pt20/Vulcan.

Table 2
Electrochemical active from cyclic voltammetry experiment with theoretical loading and loading from EDS (Pt/MWCNTs and Pt/Vulcan).

Samples	EAA ($m^2\ g^{-1}$) theoretical loading	EAA ($m^2\ g^{-1}$) EDS loading	EAA ($m^2\ g^{-1}$) Pt/Vulcan
Pt10	118	141	50
Pt20	148	151	98

where EAA is given in $cm^2\ g^{-1}$; Q in $\mu C\ cm^{-2}$; μ_{Pt} is the charge required for oxidation of a single molecule of H_2 on a polycrystalline Pt surface of 1 cm^2 (210 $\mu C\ cm^{-2}$) [31]; and L is the Pt load in the electrode (g cm^{-2}).

Table 2 shows the comparison between theoretical electroactive area with that measured on the samples. It can observe that MWCNT samples (Pt10 and Pt20) have better performance compared to the commercial catalysts (Vulcan). This is probably due to two points: 1) the use of carbon nanotubes as a support material of nanoparticles of Pt, which improve the electrical contact, and 2) highly stable Pt nanoparticles but also superior catalytic activities and durability, which may be attributed to the strengthened interactions between the Pt catalyst and the carbon nanotubes that effectively precludes migration and/or agglomeration of Pt on the carbon nanotubes support [35,36]. From these results, it becomes clear that these electrodes might be used as electrodes in PEMFC.

4. Conclusions

MWCNTs were synthesized by chemical vapor deposition method. Amorphous carbon residue and iron particles were removed from the surface of the MWCNTs with a nitric acid treatment. A colloidal dispersion of Pt was used to deposit Pt nanoparticles on the surface of the MWCNTs. The Pt nanoparticles size obtained in the colloidal dispersion was about 4.5 ± 1.9 nm. After heat treatment, Pt nanoparticles were anchored to the carbon nanotubes having a size between 6.1 ± 0.9 and 6.5 ± 1.5 nm. X-ray diffraction shows diffraction peaks corresponding to graphite and metallic Pt. Electrocatalytic activity of Pt on MWCNTs was evaluated by cyclic voltammetry the electrochemically active areas were for 118 $m^2\ g^{-1}$ for Pt10 and 148 $m^2\ g^{-1}$ for Pt20, both higher than the commercial material evaluated. The synthesized nanostructured materials based on multiwalled carbon nanotubes could be a better alternative as electrocatalysts for the proton exchange membrane fuel cells, rather than the conventional materials that use activated carbon as support.

Acknowledgments

This work was financially supported by CONACYT under project No. 116157. The authors would like to thank D. Lardizabal, E. Torres, C. Leyva, C. Ornelas, P. Pizá and W. Antúnez for their technical expertise.

References

[1] H. Karami, F. Taala, Journal of Power Sources 196 (2011) 6400–6411.
[2] M.S. Seehra, L.P. Akkineni, M. Yalamanchi, V. Singh, J. Poston, International Journal of Hydrogen Energy 37 (2012) 9514–9523.
[3] A.N. Aleshin, I.P. Shcherbakov, V.N. Petrov, A.N. Titkov, Organic Electronics 12 (2011) 1285–1292.
[4] T. Shimizu, T. Teranishi, S. Hasegawa, M. Miyake, Journal of Physical Chemistry B 107 (2003) 2719–2724.
[5] S. Meltzer, R. Resch, B. Koel, M. Thompson, A. Madhukar, A. Requicha, P. Will, Langmuir 17 (2001) 1713–1718.
[6] M. Vracar, N. Krstajic, V. Ramilovic, M. Jaksic, Journal of Electroanalytical Chemistry 587 (2006) 99–107.
[7] Y.K. Du, P. Yang, Z.G. Mou, N.P. Hua, L. Jiang, Journal of Applied Polymer Science 99 (2006) 23–26.

[8] J. Zeng, J.L. Yang, W. Zhou, Applied Catalysis A 308 (2006) 99–104.
[9] H. Wang, X. Qiao, J. Chen, X. Wang, S. Ding, Materials Chemistry and Physics 94 (2005) 449–453.
[10] B. Escobar, S.A. Gamboa, U. Pal, R. Guardián, D. Acosta, C. Magaña, X. Mathew, International Journal of Hydrogen Energy 35 (2010) 4215–4221.
[11] Z. Liua, L. Ming, L. Hong, W. Chen, J. Yang, Journal of Power Sources 139 (2005) 73–78.
[12] Y. Verde, G.A. Núñez, M.M. Yoshida, M.J. Yacamán, V.H. Ramos, A. Keer, Catalysis Today 107–108 (2005) 826–830.
[13] Y.Y. Shao, G.P. Yin, Y.Z. Gao, Journal of Power Sources 171 (2007) 558–566.
[14] A.L. Reddy, S. Ramaprabhu, Journal of Physical Chemistry C 111 (2007) 16138–16146.
[15] X. Wang, W.Z. Li, Z.W. Chen, M. Waje, Y.S. Yan, Journal of Power Sources 158 (2006) 154–159.
[16] S.J. Guo, S.J. Dong, E. Wang, Journal of Physical Chemistry C 112 (2008) 2389–2393.
[17] V. Kamavaram, V. Veedu, A.M. Kannan, Journal of Power Sources 188 (2009) 51–56.
[18] H. Kim, S.H. Moon, Carbon 49 (2011) 1491–1501.
[19] Y.S. Yun, H. Bak, H.J. Jin, Synthetic Metals 160 (2010) 561–565.
[20] B.M. Quinn, C. Dekker, S.G. Lemay, Journal of the American Chemical Society 127 (2005) 6146–6147.
[21] L. Li, Y.C. Xing, Journal of Physical Chemistry C 111 (2007) 2803–2808.
[22] Y. Yuana, J.A. Smith, G. Goenaga, D.J. Liud, Z. Luo, J. Liu, Journal of Power Sources 196 (2011) 6160–6167.
[23] M. Wang, K.D. Woo, D.K. Kim, Energy Conversion and Management 47 (2006) 3235–3240.
[24] M. Liu, J. Zhang, J. Liu, W.W. Yu, Journal of Catalysis 278 (2011) 1–7.
[25] L.H.S. Gasparotto, J.F. Gomes, G. Tremiliosi-Filho, Journal of Electroanalytical Chemistry 663 (2011) 48–51.
[26] W. Ye, H. Hu, H. Zhang, F. Zhou, W. Liu, Applied Surface Science 256 (2010) 6723–6728.
[27] R. Peña-Alonso, A. Sicurelli, E. Callone, G. Carturan, R. Raj, Journal of Power Sources 165 (2007) 315–323.
[28] Y. Peng, H. Liu, Industrial & Engineering Chemistry Research 45 (2006) 6483–6488.
[29] M. Peuckert, T. Yoneda, R.A. Dalla Betta, M. Boudart, Journal of the Electrochemical Society 133 (1986) 944–947.
[30] P. Stonehart, Journal of Applied Electrochemistry 22 (1992) 995–1001.
[31] E.F. Antunes, A.O. Lobo, E.J. Corat, V.J. Trava-Airoldi, A.A. Martin, C. Veríssimo, Carbon 44 (2006) 2202–2211.
[32] S.P. Somani, P.R. Somani, A. Sato, M. Umeno, Diamond and Related Materials 18 (2009) 497–500.
[33] M.G. Donato, S. Galvagno, G. Messina, C. Milone, A. Pistone, S. Santangelo, Diamond and Related Materials 16 (2007) 1095–1100.
[34] J. Gómez, Y. Verde, J.L. Romero, G.A. Nuñez, Fullerenes, Nanotubes and Carbon Nanostructures 17 (2009) 507–518.
[35] K. Kinoshita, P. Stonehart, J. O'M Bockris, B.E. Conway, Modern Aspects of Electrochemistry vol. 12, Plenum Press, New York, 1977.
[36] S.H. Liu, C.C. Chiang, M.T. Wu, S.B. Liu, International Journal of Hydrogen Energy 35 (2010) 8149–8154.